Controlling orbits in nonlinear vibration energy harvesters dynamics

Camille Saint-Martin*, Adrien Morel*, Ludovic Charleux*, Emile Roux* and Adrien Badel*
*Univ Savoie Mont Blanc, SYMME, F-74000, Annecy, France

Summary. Nonlinear mechanical resonators combined with piezoelectric transducers are widely used in vibration energy harvesting applications for their broadband behavior. Such nonlinear vibration energy harvesters may exhibit various orbits for a given excitation, each of them being associated with a given harvested power. Thus, in order to optimize the harvested power, it is crucial to find ways to jump from low power orbits to high power orbits, and to remain on them as long as possible. In this paper, we present a mathematical framework to test and study how effective is a given orbit jump strategy. Starting from the analytical model of a Duffing-type nonlinear mechanical energy harvester, we describe some of its dynamics, and we introduce a command function that can be used to impact the dynamics of the harvester. Thereafter, we will test and evaluate a set of command functions based on sinusoidal current injection.

Introduction

Vibrations are ubiquitous in nature and their energy can be scavenged via vibration energy harvesters (VEH) to replace batteries in low power electronic systems [1]. Nonlinear VEH have attracted the energy harvesting community because of their frequency behaviors that allow to harvest a relatively large power even if the vibration frequency shifts away from the harvester resonant frequency (for review, see e.g. [2]). However, such nonlinear VEH exhibit complex dynamical behaviors. Indeed, for a given excitation, they can oscillate on several orbits, often very different [3]. It is then necessary to find ways to stay in higher energy orbits to maximize the harvested power. For instance, [4] and [5] proposed to dynamically modify the buckling level of the VEH. [6] and [7] proposed to implement such orbit jump with a perturbation of the electrical load or with electrical impulses, respectively. While there are many existing orbit jump strategies in the literature [4, 5, 6, 7], there is a lack of mathematical framework that would allow their comparison in a unified way. In this paper, we introduce the nonlinear VEH model with an additional command function that allows to test and evaluate electrically-induced orbit jump strategies. The proposed modeling framework will allow to evaluate orbit jump strategies based on two major criteria: their potential for orbit jump and their energy consumption.

Electromechanical dynamics nonlinear vibration energy harvesters

A vibration energy harvester usually involves 3 sub-systems: a mechanical resonator, an electronic energy extraction circuit and a storage unit. In this study, we focus on the Duffing-type resonator and the influence of the extraction circuit on its dynamical behavior. A complete scheme of the system is given in Fig.1(a). The resonator consists of buckled steel beams on which a proof mass M is fixed. A piezoelectric transducer is used for mechanical-to-electrical energy conversion. It has a force factor α and a blocked capacitance C_p. The piezoelectric element is connected to the extraction circuit drawing an electrical current i. The piezoelectric voltage is noted v. The harvested power corresponds to the one collected in the electronic extraction circuit connected to the piezoelectric element.

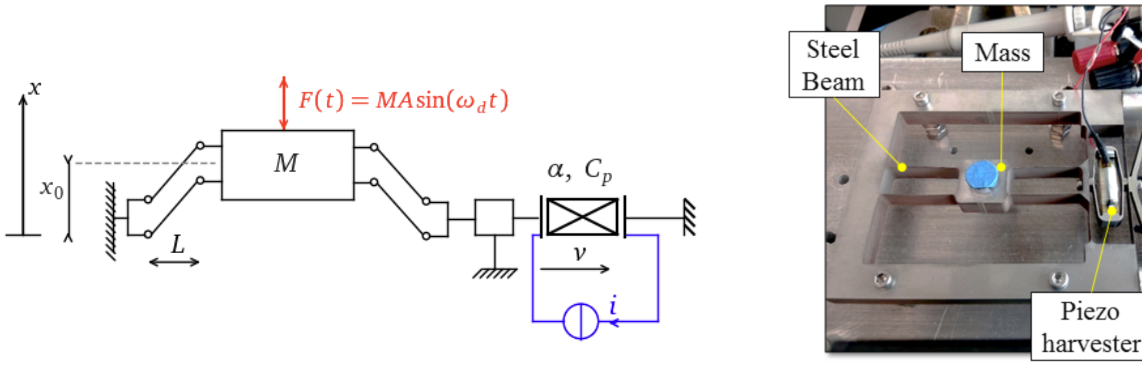

(a) (b)

Figure 1: (a) Schematic of the vibration energy harvester (b). Experimental prototype of a Duffing-type VEH [8].

The electromechanical dynamics of this nonlinear VEH can be modeled as follows:

$$\begin{cases} \ddot{x} = -\dfrac{\omega_0^2}{2}\left(\dfrac{x^2}{x_0^2} - 1\right)x - \dfrac{\omega_0}{Q}\dot{x} - 2\dfrac{\alpha}{ML}xv + A\sin(2\pi f_d t) \\ \dot{v} = 2\dfrac{\alpha}{LC_p}x\dot{x} - \dfrac{1}{C_p}i \end{cases} \tag{1}$$

where x is the position of the mass M. The resonator presents two stable positions at $x = \pm x_0$ (each corresponding to a

local minimum of the elastic potential energy and associated with a potential well). From the linearized behavior obtained from small oscillations around $x \approx x_0$, a natural angular frequency ω_0 and a mechanical quality factor $Q > 0$ can be found. The resonator is submitted to a sinusoidal ambient acceleration of amplitude A and frequency f_d. The nonlinear ordinary differential equations (1) were numerically solved for different vibration frequency values f_d and from different initial states $\boldsymbol{X}(0) = \begin{pmatrix} x^0 & \dot{x}^0 & v^0 \end{pmatrix}^\top$. Each simulation was performed until convergence to a periodic or a chaotic regime. The orbits were deduced and classified by type (periodic or chaotic) and, when periodic, by their harmonic or subharmonic order. These subharmonic orbits correspond to the case where the mass oscillates at a frequency which is a submultiple of the vibration frequency. An orbit is high when the mass oscillates around the two stable equilibrium positions. On the other hand, an orbit is low when the mass oscillates around one of the two stable equilibrium positions. In this paper, we take the following notations: H1H (resp. H1L) for a first order high (resp. low) harmonic and SH5H (resp. SH5L) for a fifth order high (resp. low) subharmonic. In the case where the electronic circuit is a simple resistor $R = 7.8$ kΩ, the current is given by $i = v/R$. The average harvested power corresponds to the power dissipated in the resistor and can be computed by calculating the mean value of $v.i = v^2/R$.

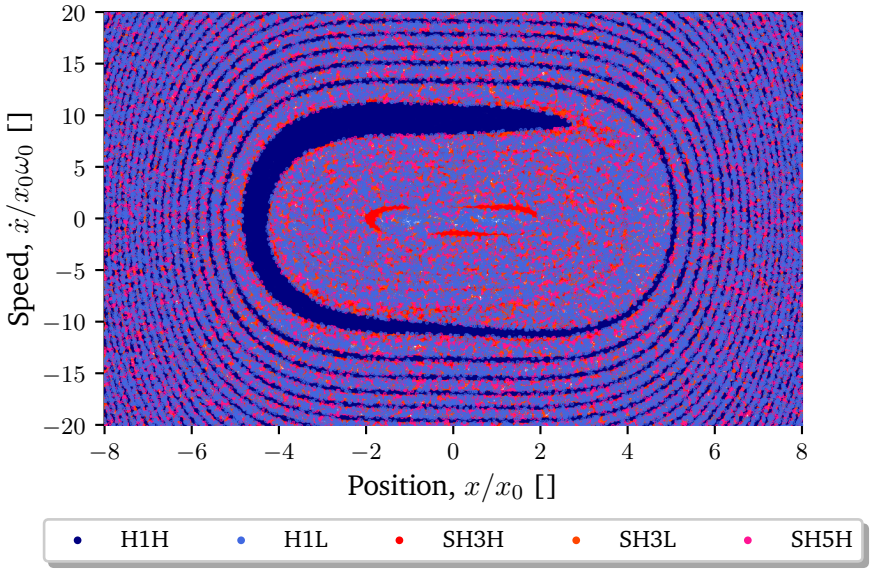

Figure 2: Basins of attraction for $f_d = 50$ Hz with a grid of 400 000 starting points [9].

The basins of attraction of the bistable (for $f_d = 50$ Hz) are shown in Fig.2. As seen in Fig.2, for a given vibration frequency and for some initial conditions, one can start on a low energy orbit. For example, at $f_d = 50$ Hz the system can start on H1L, SH3L, SH5H, SH3H or H1H (best case), and when the system stabilizes on H1L it is interesting to perturb the system by means of an orbit jump strategy in order to converge to a highest orbit (SH3L, SH5H, SH3H or H1H). In Fig.3, we can observe that multiple orbits of various powers coexist for a given vibration frequency. The longer one stays on highest power orbits, the better the performance. The goal of our study is to define a command function i_u that enables to jump from low power orbits to high power orbits. [1]

Dynamics adjustment by current injection

One way to induce such orbit jump is to dynamically modify one of the state-variable of the electromechanical system (i.e., x, $\dot{x}$ or v). From a practical point of view, it is much easier to implement a change of v than a change of x or $\dot{x}$, thanks to an adaptive electrical circuit. To modify the piezoelectric voltage v and to avoid any voltage discontinuities, we add an injection current i_u to the load current i_L. In this case, the total current flowing in the piezoelectric material i is given by $i = i_L - i_u$. We then end up with an optimal control problem where the output to control is the orbit and the command function is the injected current $i_u : t \mapsto \mathbb{R}$ which is assumed to be a continuous piecewise function.

[1] In this analysis the jump from chaotic orbits (present around 25 Hz, see Fig.3) will not be discussed.

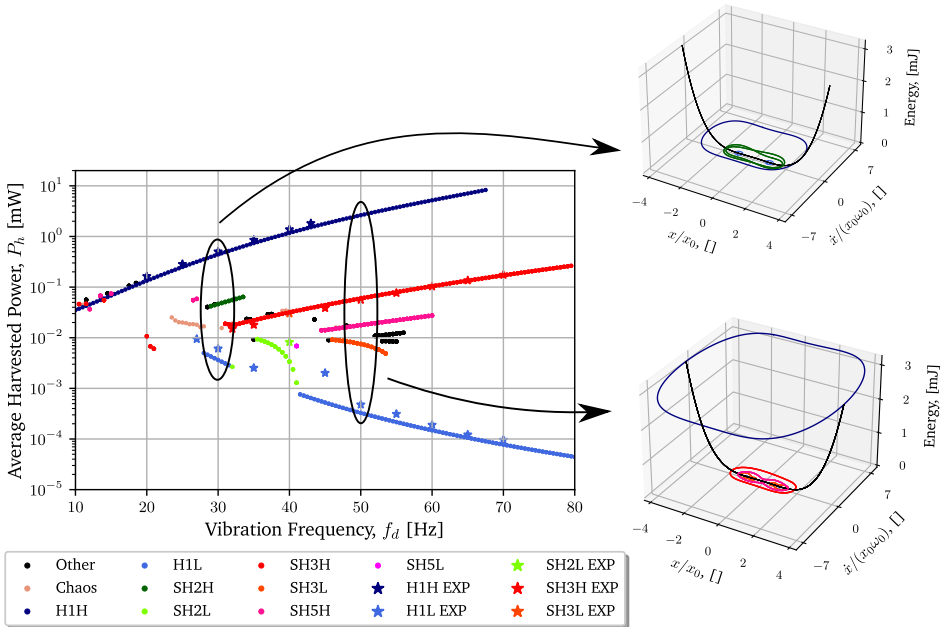

Figure 3: Simulated average harvested power as a function of the vibration frequency f_d for the different existing orbits [9].

$$\begin{cases} \ddot{x} = -\dfrac{\omega_0^2}{2}\left(\dfrac{x^2}{x_0^2}-1\right)x - \dfrac{\omega_0}{Q}\dot{x} - 2\dfrac{\alpha}{ML}xv + A\sin(2\pi f_d t) \\ \dot{v} = 2\dfrac{\alpha}{LC_p}x\dot{x} - \dfrac{1}{C_p}i_{\mathrm{L}} + \dfrac{1}{C_p}i_u \\ \dot{E} = \dfrac{2\alpha}{L}x\dot{x}v - C_p v\dot{v} = v.i = v.i_{\mathrm{L}} - v.i_u \\ \boldsymbol{X}(0) = \begin{pmatrix} x^0 & \dot{x}^0 & v^0 \end{pmatrix}^\top \end{cases} \tag{2}$$

Where E is the total harvested energy. The instantaneous harvested power $\dot{E}$ can be calculated from the power consumption of the load $v.i_{\mathrm{L}} \geq 0$ minus the injected power $v.i_u$. If we control the injected current function i_u, we can change the trajectory $t \mapsto \boldsymbol{X}(t)$ by punctually modifying the piezoelectric voltage v. Starting from this mathematical framework, the next section will present the analysis and evaluation of electrically-induced orbit jump strategies.

Results and discussion

We define a command function that consists in injecting a sinusoidal current at a certain time t_0. This injected current presents an amplitude I_e, a phase shift ψ_e with respect to the ambient excitation and an angular frequency ω_e. Moreover, the current is injected for a duration Δt, such as the orbit jump stops at $t_0 + \Delta t$. Since the excitation of the system is harmonic, we define dimensionless parameters k_{t_0} and $k_{\Delta t}$ as follows: $k_{t_0} = t_0/T_d$ and $k_{\Delta t} = \Delta t/T_d$. Therefore, there are five influence orbit jump parameters $(k_{t_0}, k_{\Delta t}, I_e, \psi_e, \omega_e)$ to study.

$$i_u(t) = \begin{cases} I_e \sin(\omega_e t + \psi_e), & \text{for } t/T_d \in [k_{t_0}, k_{t_0} + k_{\Delta t}] \\ 0, & \text{otherwise} \end{cases} \tag{3}$$

To analyze the effectiveness of this orbit jump technique consisting in the injection of current (3), we start on a low energy orbit. Thereafter, we simulate different combinations of $(k_{t_0}, k_{\Delta t}, I_e, \psi_e, \omega_e)$ and analyze their influence on the dynamics of the harvester. Figure 4 presents an example of the orbit jump strategy for $f_d = 50$ Hz with arbitrary parameter values $(k_{t_0}, k_{\Delta t}, I_e, \psi_e, \omega_e) = (0.35, 2.5, 0.18, 1.6\pi, 2\omega_d)$. Figure 4(a) shows the corresponding injected current waveform (3) during the first few periods and after 1 000 periods. At the beginning of the simulation, the system oscillates on the lowest existing orbit (H1L) during 5 vibration periods T_d. For $t = (5 + k_{t_0})T_d = 5.35T_d$, the orbit jump strategy using the injected current described in Fig.4(a) is applied for a duration of $\Delta t = 2.5T_d$. Fig.4(b,c) show that there is no transient and the VEH converges almost directly to the H1H steady state (green and red curves). This convergence is similar to the one obtained with a buckling level modification (see [4, 5]).

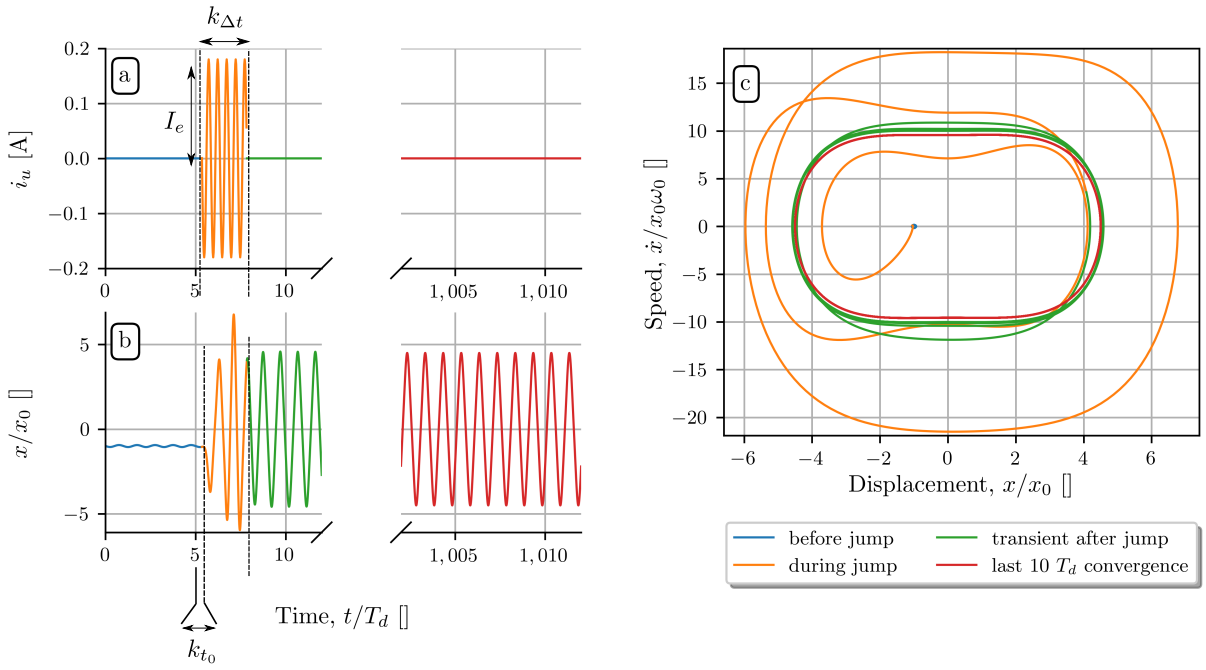

Figure 4: (a) Sinusoidal injected current (3) as a function of time with parameter values $(k_{t_0}, k_{\Delta t}, I_e, \psi_e, \omega_e) = (0.35, 2.5, 0.18, 1.6\pi, 2\omega_d)$, (b) displacement as a function of time for $f_d = 50$ Hz before (H1L in blue), during (in orange) and after (in green and red) the orbit jump. (c) Trajectory in the dimensionless phase plane $(x/x_0, \dot{x}/x_0\omega_0)$.

The invested energy during the orbit jump E_{inv} (4) consists in the integral of the instantaneous harvested power subtracted from the instantaneous injected power over the jump duration. (5) computes total injected energy during the orbit jump, considering both the current flowing in the piezoelectric material and the current flowing in the load R.

$$E_{\text{inv}} = \int_{t_0}^{t_0+\Delta t} \left[v(t).i_u(t) - v(t).i_L(t)\right] dt \tag{4}$$

$$E_{\text{inj}} = \int_{t_0}^{t_0+\Delta t} v(t).i_u(t)dt = E_{\text{inv}} + \int_{t_0}^{t_0+\Delta t} v(t).i_L(t)dt \tag{5}$$

Thereafter, an evolutionary algorithm inspired from natural selecting process [10, 11] is used for investigating optimal orbit jump parameters $(k_{t_0}, k_{\Delta t}, I_e, \psi_e, \omega_e)$ that belong to $[0,1] \times [0,50] \times [0,0.2] \times [0,2\pi] \times [0,4\omega_0]$ where $\omega_0 = 121$ rad.s^{-1}. Using the glossary of evolutionary strategies, the *population* is an orbit jump parameters (*individuals*) collection, the *fitness* corresponds to the objective function value that is the total injected energy (5) under the constraint that individuals have converged to the targeted orbit (of higher energy than the initial orbit). The best 10% of individuals are selected for the next generation and the classic operations of crossing (single point crossover) and mutation are applied. By means of evolutionary strategy, optimum orbit jump parameters values are obtained at 50 Hz: $(k_{t_0}^{\text{opt}}, k_{\Delta t}^{\text{opt}}, I_e^{\text{opt}}, \psi_e^{\text{opt}}, \omega_e^{\text{opt}}) = (0.80, 2.08, 0.04, 2.49, 415.34)$.

Running simulations with identical initial condition $\boldsymbol{X}(0)$ that belongs to the basin of attraction of the H1L at 50 Hz and taking $(k_{t_0}, k_{\Delta t}, I_e, \psi_e, \omega_e)$ in $\{k_{t_0}^{\text{opt}}\} \times \{k_{\Delta t}^{\text{opt}}\} \times [0, 0.2] \times [0, 2\pi] \times \{\omega_e^{\text{opt}}\}$ gives Fig.5 scatter plot $(\psi_e/2\pi, I_e)$. Note that, if the injected current amplitude I_e is almost zero, the injection of current is too low and the system remains stuck on the initial orbit H1L (light blue area in the bottom of Fig.5). To jump from H1L to SH3H (resp. H1H), it is necessary to consider the parameter values that are associated with red (resp. dark blue) areas in Fig.5 (for example, area in the upper right (resp. in the middle left)). Arrows in Fig.5 give examples of parameters combinations (materialized by stars) assuring jump from H1L to H1H, SH3H and SH3L, respectively. Generally, the injected current amplitude increases with the energy level of the targeted orbit. For example, in order to reach H1H when starting from H1L, the value of I_e needs to be higher than those to reach SH3L or SH5H.

Figure 6 presents this optimal orbit jump solution parameters obtained by using the aforementioned algorithm. Figure 6(a) shows that the injected current is applied on a relatively short instant. Note that the injection of current is stopped when the VEH is in the neighbourhood of the basin of attraction of H1H.

For each initial orbit, optimum orbit jump parameters that allow to reach the highest energy orbit are found by means of aforementioned algorithm. Table 1 gives invested energy values associated with optimal orbit jump parameters for jumping from a given initial orbit to a given targeted orbit for $f_d = 47$ Hz. For example, invested energy required to jump from H1L to H1H is 2.54 mJ. Table 1 underlines, for some frequencies, the interest of jumping in "k-times" ($k > 1$, integer), i.e., in k low cost jumps. As a matter of example, for jumping from H1L to H1H, one might imagine jumping from H1L to SH3L, to SH5H, to SH3H, then to H1H. The sum of the invested energies associated to each step is equal to 1.79 mJ, which is lower than the invested energy for jumping directly from H1L to H1H (2.54 mJ).

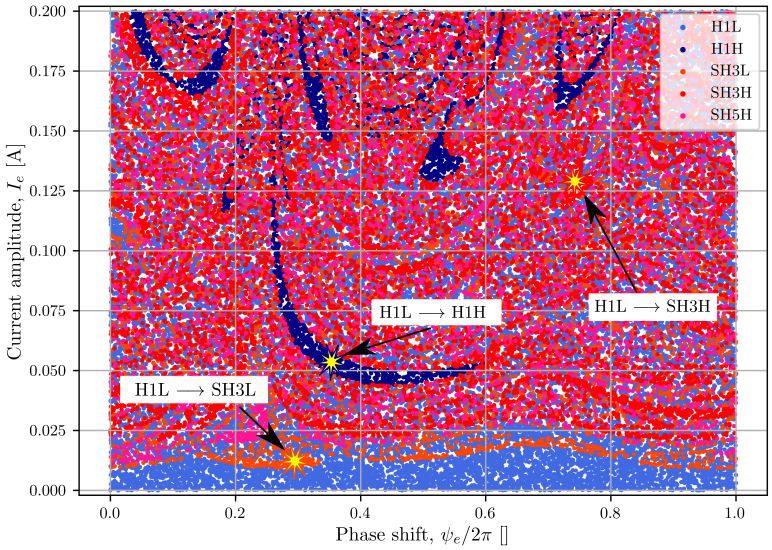

Figure 5: Map $(k_{t_0}^{\text{opt}}, k_{\Delta t}^{\text{opt}}, I_e, \psi_e/2\pi, \omega_e^{\text{opt}})$ starting from H1L for $f_d = 50$ Hz. Arrows from left to right illustrate candidate values for $(\psi_e/2\pi, I_e)$ in order to jump from H1L to SH3L, from H1L to H1H or H1L to SH3H. The map has been computed with 50 000 quintuplets $(k_{t_0}^{\text{opt}}, k_{\Delta t}^{\text{opt}}, I_e, \psi_e, \omega_e^{\text{opt}})$ where $(I_e, \psi_e) \in [0, 0.2] \times [0, 2\pi]$.

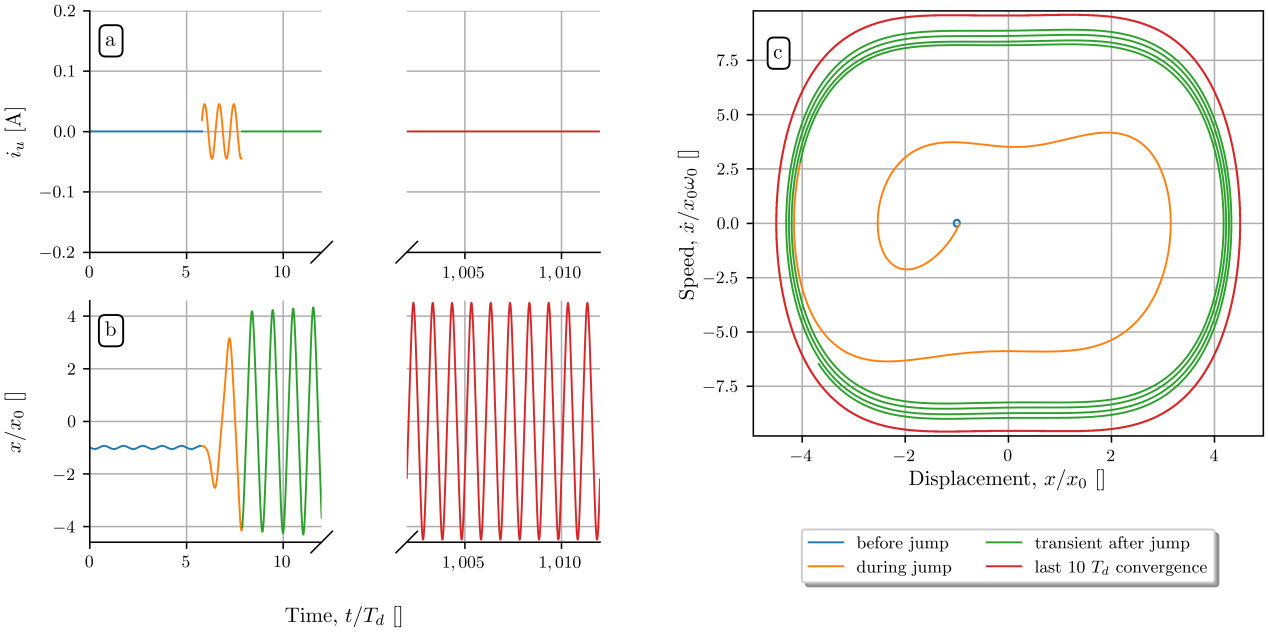

Figure 6: (a) Sinusoidal injected current (3) as a function of time with optimal parameter values $(k_{t_0}^{\text{opt}}, k_{\Delta t}^{\text{opt}}, I_e^{\text{opt}}, \psi_e^{\text{opt}}, \omega_e^{\text{opt}}) = (0.80, 2.08, 0.04, 2.49, 415.34)$. (b) Displacement as a function of time for $f_d = 50$ Hz before (H1L in blue), during (in orange) and after (in green and red) the optimized orbit jump. (c) Trajectory in the dimensionless phase plane $(x/x_0, \dot{x}/x_0\omega_0)$.

Figure 7 shows the optimal invested energy required to jump from the lowest existing orbit to H1H (resp. SH3H) as a function of the vibration frequency. Note that there are few values of the invested energy required for jumping on the two targeted orbits (H1H and SH3H) for vibration frequencies below 25 Hz because there is almost only H1H in this vibration frequency range. Figure 7 shows that the invested energy increases with the vibration frequency[2]. Moreover, this orbit jump strategy makes it possible to reach H1H from the lowest existing orbit until its cutoff frequency at 67 Hz. Note that, the optimal amplitude I_e^{opt} necessarily increases with the vibration frequency and the energy level of the targeted orbit.

[2]Indeed, the displacement of H1H becomes larger with the vibration frequency, which explains why the energy gap between H1H and H1L becomes wider [9].

Initial orbit \ Targeted orbit	SH3L	SH5H	SH3H	H1H
H1L	5.10^{-3}	1.10^{-2}	$3.7.10^{-2}$	2.54
SH3L	0	7.10^{-3}	$1.8.10^{-2}$	2.06
SH5H		0	3.10^{-2}	2.08
SH3H			0	1.75

Table 1: Optimal invested energy (4) (mJ) required to jump from an initial orbit (left column) to a targeted orbit (top row) for $f_d = 47$ Hz. Invested energy values for jumping from H1L to H1H with 4 intermediates jumps are colored in red while the invested energy for jumping from H1L to H1H in one time is colored in blue.

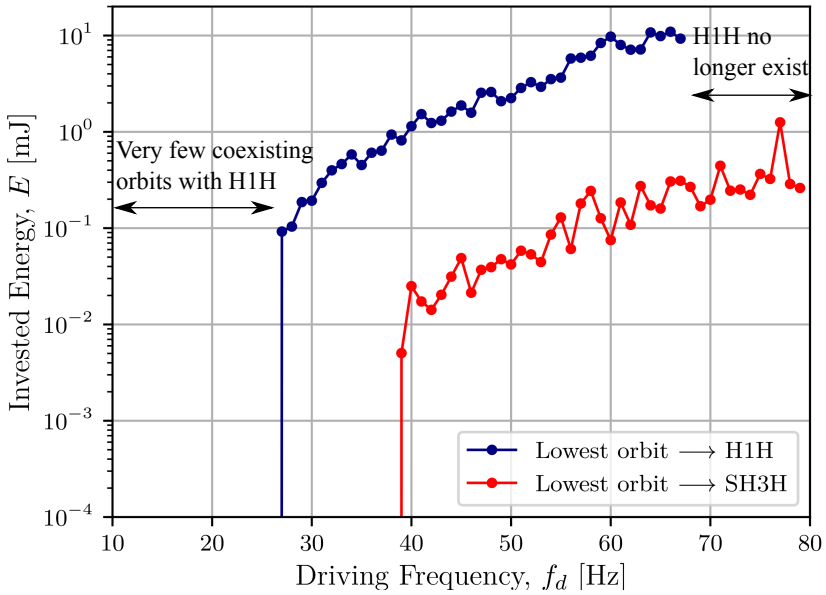

Figure 7: Evolution of the optimal invested energy required to jump from the lowest existing orbit to H1H (in blue) and those to jump from the lowest existing orbit to SH3H (in red) as a function of the vibration frequency.

Conclusion

In the present paper, we proposed a mathematical framework in order to analyze and evaluate electrically-induced orbit jump strategies. From this framework, we studied an orbit jump approach based on a sinudoidal injected current. By means of an evolutionary algorithm, the optimal set of parameters of this orbit jump approach has been determined. Among results of this analysis is that the optimal injection current that minimizes the injected energy is relatively short and stopped when the VEH is in the neighbourhood of the basin of attraction of the targeted orbit. Another insights is that, for some frequencies, the injected current consumes less energy to jump from a low energy orbit to a high energy orbit with multiple small jumps instead of a single large jump. In the future, the proposed framework could be used to find the optimal orbit jump strategy with a generic current waveform with many additional degrees of freedom.

Acknowledgements

This project has received funding from the European Union's Horizon 2020 research and innovation program under grant agreement No 862289.

References

[1] Sezer N., Koç M., (2021) A comprehensive review on the state-of-the-art of piezoelectric energy harvesting. *Nano Energy* https://doi.org/10.1016/j.nanoen.2020.105567

[2] Jia Y., (2020) Review of nonlinear vibration energy harvesting: Duffing, bistability, parametric, stochastic and others, *Journal of Intelligent Material Systems and Structures* https://doi.org/10.1177/1045389X20905989

[3] Lansbury A.N., Thompson J. M. T., Stewart H. B., (1992) BASIN EROSION IN THE TWIN-WELL DUFFING OSCILLATOR. *International Journal of Bifurcation and Chaos* https://doi.org/10.1142/S0218127492000677

[4] Huguet T., Lallart M., Badel A., (2019) Orbit jump in bistable energy harvesters through buckling level modification. *Mechanical Systems and Signal Processing*, **128**:202–215 https://doi.org/10.1016/j.ymssp.2019.03.051

[5] Huang Y., Liu W., Yuan Y., Zhan Z., (2020) High-energy orbit attainment of a nonlinear beam generator by adjusting the bukling level. *Sensors and Actuators A: Physical*, **312**:112164 https://doi.org/10.1016/j.sna.2020.112164

[6] Wang J., Liao W.-H., (2019) Attaining the high-energy orbit of nonlinear energy harvesters by load perturbation. *Energy Conversion and Management* https://doi.org/10.1016/j.enconman.2019.03.075

[7] Udani J. P., Arrieta A. F., (2017) Sustaining high-energy orbits of bi-stable energy harvesters by attractor selection. *Applied Physics Letters 111* https://doi.org/10.1063/1.5000500

[8] Huguet T., (2018). Vers une meilleure exploitation des dispositifs de récupération d'énergie vibratoire bistables : Analyse et utilisation de comportements originaux pour améliorer la bande passante. Ph.D. thesis. https://tel.archives-ouvertes.fr/tel-01957377

[9] Saint-Martin C., Morel A., Charleux L., Roux E., Benhemou A., Badel A., (2022). Power expectation as a unified metric for the evaluation of vibration energy harvesters. *Mechanical Systems and Signal Processing*. https://doi.org/10.1016/j.ymssp.2022.109482

[10] Sivanandam S., Deepa S., (2008). Genetic Algorithms. In: Introduction to Genetic Algorithms. *Springer*. https://doi.org/10.1007/978-3-540-73190-0_2

[11] Konak A., Coit D. W., Smith A. E., (2006). Multi-objective optimization using genetic algorithms: A tutorial. *Reliability Engineering & System Safety*, https://doi.org/10.1016/j.ress.2005.11.018